Journal of Computational Electronics (2018) 17:1790–1796
https://doi.org/10.1007/s10825-018-1229-2

Ion shot noise in Hodgkin–Huxley neurons

Beatriz G. Vasallo[1] · **Javier Mateos**[1] · **Tomás González**[1]

Published online: 9 August 2018

Abstract
Ion shot noise, the noise associated to the random passage of ions across the cell membrane, is studied by means of a stochastic model based on the Hodgkin–Huxley equations, which includes gating channels for sodium and potassium cations and leakage channels through the biological membrane. Apart from shot noise, other sources such as extrinsic and channel noise are taken into account. Ion shot noise, of increasing influence for smaller membrane patch sizes S, can lead to the emergence of action potentials in the membrane voltage in the presence of sinusoidal excitation currents below the threshold for the onset of spikes. The spiking activity in the presence of noise has been analyzed in terms of the coefficient of variation CV, the inter-spike interval histogram, the spectrum of membrane voltage fluctuations and the signal-to-noise ratio SNR. CV shows improved coherence in the sequence of randomly generated spikes due to the presence of shot noise. The voltage noise spectra show a common signature of the presence of spikes under different operating conditions, even in the absence of excitation. The SNR exhibits intrinsic stochastic resonance when varying S. For a sinusoidal excitation current with amplitude 1.5 μA/cm^2 and frequency 50 Hz, the SNR presents optimal values around 0.2 μm^2. When considering the presence of ambient noise in the excitation current, extrinsic stochastic resonance is found for $S > 0.6$ μm^2.

Keywords Ion shot noise · Hodgkin–Huxley equations · Cell membrane

1 Introduction

Bio-inspired electronic devices and neuromorphic architectures mimicking the naturally efficient brain functionality [1–7] require physical models that further assist the knowledge of the human brain. The essential physical properties of neurons and axons are related to the electric behavior of their membrane [6–9], whose time evolution is typically modeled by means of the phenomenological Hodgkin–Huxley (HH) equations [10]. The HH model accounts for the equilibrium conditions and the action potential, which is a potential spike, activated by sufficient external current I_{app}, consisting of a sharp increase followed by a short inversion of the cell membrane voltage V_m. As nonlinear systems that can evolve from a threshold, in biological membranes random noise can improve the detection of weak signals by enhancing them in a correlated fashion over the threshold, leading to the well-known stochastic resonance (SR), repeatedly demonstrated in sensory neuronal systems (see Refs. [11–13] as examples).

To assist the design of neuro-inspired hardware, as well as to explore the noise behavior of the cell membrane, we propose a stochastic solver of the HH equations that includes ion shot noise among other noise sources. As an alternative to over-detailed and computationally demanding kinetic molecular simulators [14–18], our model avoids the consideration of spatial distributions of channels and co-transporters at a molecular level. Instead, ion channels assemblies are described as a whole by means of a continuous model [19]. The main goal of this work is to analyze the current fluctuations provoked by the random dynamics of the ions crossing through the cell membrane and evaluate their influence on the spike generation when considered as the only noise source. Ion shot noise is typically considered as negligible when other electrical sources of neural noise are taken into account [20–25], in particular ion channel noise, whose influence also increases when reducing the size of the membrane patch S [20]. However, the study of shot noise in ion channels is relevant by itself due to the

✉ Beatriz G. Vasallo
bgvasallo@usal.es

Javier Mateos
javierm@usal.es

Tomás González
tomasg@usal.es

[1] Dpto. Física Aplicada, Universidad de Salamanca, Plaza de la Merced s/n, 37008 Salamanca, Spain

information it can provide about ion dynamics in biological membranes [19, 26, 27] and its possible influence on the analysis of channels with very fast gating [28].

In the presence of periodic stimulus, internal ion shot noise can originate voltage spikes with a signal-to-noise ratio (SNR) exhibiting intrinsic SR, this is, SR versus decreasing patch area (increasing shot noise). When adding external noise, extrinsic SR is also observed versus the noise strength. In order to evidence these size-related effects, realistic values of S ranging from 100 to 0.1 μm^2, jointly with less-realistic smaller sizes, have been considered. For the larger S, shot noise is practically negligible; its influence can be significant when approaching $S=1$ μm^2, which approximately corresponds to the patch size of brain synapses. For $S=0.1$ μm^2, as in sub-synaptic compartments, the present continuous model starts losing validity due to the small number of ion channels. However, even if a discrete consideration of the channels becomes necessary, smaller values of S have been also analyzed in order to go deeply into the effect of increased levels of ion shot noise.

2 Physical model

The cell membrane can be considered as an insulator separating intracellular and extracellular spaces, which are electrolytes containing sodium (Na^+) and potassium (K^+) cations. Ion leakage and voltage-gated channels connect both spaces through the membrane. Voltage-gated channels, specific for each type of ion, are opened or closed depending on the voltage across the cell membrane $V_m(t)$. In accordance with HH model [10], the electrical time evolution of the cell membrane is described in terms of $V_m(t)$, linked to the ion currents crossing the membrane. It evolves due to the so-called gating variables, $m(t)$, $h(t)$ and $n(t)$, which determine the opening or the closing of sodium and potassium channels.

Thus, the cell membrane can be considered as a capacitance C_m, which is charged/discharged by the currents crossing it, as

$$C_m \frac{dV_m(t)}{dt} = I_{app} - (I_{Na} + I_K + I_{leak}), \quad (1)$$

where I_{app} is an external excitation current density, which can initiate a voltage spike; and I_{ion}, with the suffix ion = Na, K or leak, is the current density due to sodium cations, potassium cations or ion leakage (mainly chloride anions), respectively. $I_{ion} > 0$ when positive charge leaves the cell, and $I_{ion} < 0$ in the opposite case. In order to solve the HH equations, a straightforward Monte Carlo code including shot noise in a natural way has been developed, as detailed in Section 2.1 of Ref. [19]. In this model, based on the HH expressions for I_{ion} [10], we consider independent probabilities for each ion to cross the cell membrane and make use of the Gillespie method [29, 30] to account for their stochastic transmembrane kinetics. Assuming that the crossing of ions is a memoryless process, the time between two consecutive passages is calculated following Poisson statistics. In this way, I_{ion} contains the fluctuations associated to the random passage of ions through the cell membrane (shot noise) and such fluctuations are incorporated into the evaluation of $V_m(t)$ when solving Eq. (1). Details of the model and related parameters can be found in Ref. [19].

When $I_{app}=0$, the average value of $V_m(t)$ is the so-called resting potential, about -68 mV; the HH model assumes that it is zero for simplicity, as done in this work. For an appropriate I_{app} driving the membrane potential beyond a given threshold, a potential spike (action potential) appears in $V_m(t)$. At the onset of the spike, sodium channels open and a negative I_{Na} emerges due to the entering of Na^+ into the intracellular space, which leads to a further increase in V_m. Potassium channels need higher V_m than sodium ones to open, which occurs due to the appearance of I_{Na}. The exit of potassium ions leads to a positive I_K. Sodium channels start closing when V_m reaches a maximum value; once closed, they remain locked until the equilibrium is recovered, which prevents any new spike. This is the so-called refractory period, during which potassium channels are still open for leaving K^+ cations, leading to a decrease in V_m, which, in turn, causes the further closing of such potassium channels and the recovering of the resting conditions [19]. The refractory period, of the order of 10–20 ms, imposes an intrinsic rhythm in the internal spike activity by avoiding the onset of further action potentials until it finishes [21]. Once any I_{app} ceases, $V_m(t)$ recovers the resting value.

Sinusoidal current densities are applied as external excitation signals

$$I_{app}(t) = I_A \sin(2\pi f t). \quad (2)$$

For the analysis, we will consider a signal with frequency $f=50$ Hz and amplitude $I_A=1.5$ $\mu A/cm^2$, which drives the membrane voltage very close to the threshold for the onset of spikes. To include the presence of external noise, a term $\eta(t)$ can be added at the right hand side of Eq. (2), modeled as a Gaussian white noise source with autocorrelation function [20]

$$\langle \eta(t)\eta(t') \rangle = 2 \cdot D_{ext} \cdot \delta(t - t'), \quad (3)$$

where D_{ext} is the external noise strength.

To complete our analysis, at the final part of the work we have also considered the presence of ion channel noise modeled by considering the Langevin generalization for the HH equations, as in [20].

The equations are solved in time domain by means of the standard Euler algorithm with a time step $\Delta t = 2\ \mu$s [19, 20]. After 10 ms in the absence of excitation (to ensure initial equilibrium conditions), the signal is applied during a time multiple of the driving period.

The existence of a voltage spike at a given moment t in the stochastic voltage signal $V_{\rm m}(t)$ is discerned when upward-crossing a detection threshold value $V_0 = 60$ mV, having previously taken values below $V_{\rm f} = 20$ mV. Other values of V_0 and $V_{\rm f}$ within a reasonable range can be used providing essentially the same results. Once detected the times of the spike occurrences t_i, the corresponding spike train function is given by

$$u(t) = \sum_{i=1}^{N} \delta(t - t_i), \tag{4}$$

where N is the total number of spikes taking place during the simulation time.

In order to analyze the noise behavior of the system, the inter-spike interval histogram (ISIH), directly calculated from $u(t)$, the coefficient of variation (CV) and the signal-to-noise ratio (SNR) are evaluated.

The spike train coherence is measured by CV, defined as [20]

$$\mathrm{CV} = \frac{\sqrt{\langle T \rangle^2 - \langle T \rangle^2}}{\langle T \rangle}, \tag{5}$$

where $\langle T \rangle$ and $\langle T \rangle^2$ are, respectively, the mean and the mean-squared values of inter-spike intervals. N must be high enough for a proper calculation of CV. For a fully incoherent sequence, corresponding to a spike train following Poisson statistics, CV = 1. When dealing with ion shot noise, this is the tendency for the bigger patches.

For a given $u(t)$, the corresponding power spectral density $S_U(f)$ contains abrupt peaks localized at multiples of the driving frequency superimposed on a broadband background. The SNR is calculated as the ratio between the peak value at the driving frequency (with respect to the background noise) and the background power spectrum [20]. In addition to $u(t)$, the spectral analysis of the fluctuations of $V_{\rm m}(t)$ is also of interest [23, 31].

3 Results and discussion

When $I_{\rm app}$ consists of a sinusoidal signal with amplitude and frequency such that $V_{\rm m}$ is driven close to the action potential threshold, ion shot noise can play a significant role on the onset of spikes, otherwise absent in a deterministic case (without any noise source). Figure 1 illustrates such a case. It presents the time evolution of $V_{\rm m}(t)$ (a) in the absence of any external excitation, and (b) in response to an excitation $I_{\rm app}$ with $I_{\rm A} = 1.5\ \mu$A/cm^2 and $f = 50$ Hz, for a membrane patch size $S = 1\ \mu$m^2, in the presence of shot noise as only noise source. In Fig. 1b, the deterministic solution has been also plotted for comparison. In the absence of $I_{\rm app}$, the excursions of $V_{\rm m}$ originated by shot noise are not strong enough for the onset of action potentials. The same happens when $I_{\rm app}$ is present in the absence of shot noise. In contrast, when shot noise and $I_{\rm app}$ are considered simultaneously in the simulation, about 35% of the periods of the applied signal lead to spikes (unevenly distributed in time), taking place slightly after the maximum in $I_{\rm app}(t)$.

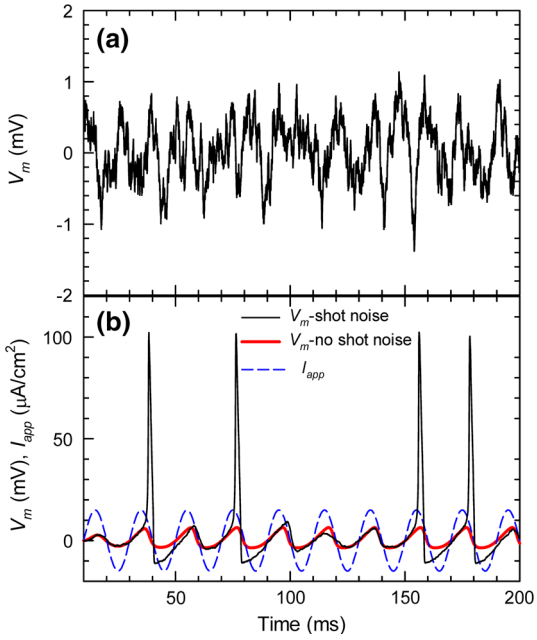

Fig. 1 Time evolution of **a** $V_{\rm m}$ in the absence of any external excitation and **b** $V_{\rm m}$ and $I_{\rm app}$ for $I_{\rm A} = 1.5\ \mu$A/cm^2 and $f = 50$ Hz, when ion shot noise is considered as the only noise source in the system. $S = 1\ \mu$m^2. In (**b**), the deterministic solution is also plotted for comparison

In order to study the coherence in the spike train $u(t)$, CV is plotted in Fig. 2 as a function of S for the same excitation as in Fig. 1b. The case $I_{\rm app} = 0$ is also plotted for comparison. The simulation time is 200 s, which ensures a large enough number of spikes N for an appropriate evaluation of CV, even for the bigger patches. In the realistic range $S > 0.1\ \mu$m^2, when increasing S, CV growths from values around 0.6–1 because the appearance of spikes originated by shot noise becomes not only less frequent but also more incoherent. The smooth valley appearing in CV in the range $1\ \mu\text{m}^2 < S < 10\ \mu\text{m}^2$ can be associated to the transition presence/absence of inter-spike intervals coinciding with one period of the external signal, as will be discussed later. For decreasing S below $0.1\ \mu$m^2, the increase in shot noise strength leads to a higher number of spikes more regularly distributed in time, so that CV decreases down to optimal

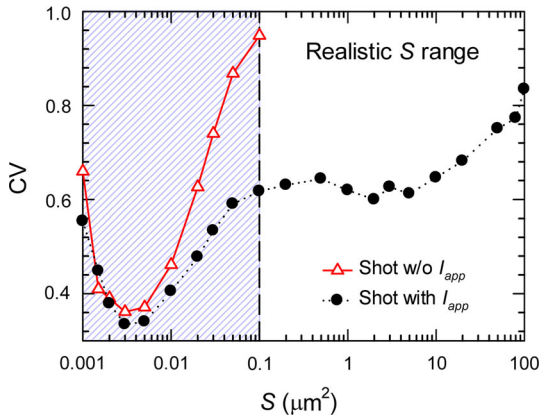

Fig. 2 CV as a function of S for a sinusoidal excitation with I_A=1.5 μA/cm^2 and f=50 Hz when ion shot noise is considered as the only noise source in the system. The case I_{app}=0 is also plotted for comparison. The non-realistic range of S is shaded for clarity

values for S around 0.003 μm^2. For smaller values of S, CV growths again because of a so high level of noise that the coherence of the spike sequence is lost. Thus, even if for unrealistic values of S, a resonance in CV emerges associated to ion shot noise within the model used.

In the absence of any external I_{app}, shot noise by itself is not strong enough to provoke the appearance of spikes for $S>0.1$ μm^2. However, for lower S, a resonance, very similar to that found in the presence of shot noise, is found in CV. This fact indicates that, although the sinusoidal I_{app} induces a reduction in CV in comparison with the case I_{app}=0, for the lower values of S, shot noise makes visible a rhythm in the spiking activity, related to the internal dynamics of the system, that dominates over any external signal. Very similar results are found in Ref. [20] for the case of channel noise, another source of internal noise.

In order to further illustrate the intrinsic coherence in $u(t)$, Fig. 3a–f presents the ISIH for the same sinusoidal excitation and several values of S ranging from 100 to 0.003 μm^2. The corresponding results for I_{app}=0 are also plotted for comparison. In all cases, the total simulation time is 200 s. For realistic values of S ($S>0.1$ μm^2), the spiking activity is dominated by the rhythm of the external signal, since the spikes always take place slightly after the maximum values of I_{app} (see Fig. 1b). Thus, the spikes are distributed around multiples of the signal period. For S=100 μm^2 (Fig. 3a), shot noise originates so few spikes that they are nearly incoherent. For 10 μm^2 (Fig. 3b), the shot noise level is still low and I_{app} induces spikes randomly sequenced in time intervals that are at least two periods of the signal. This happens because, when a spike occurs, its refractory period overlaps the following maximum of the periodic external signal and the threshold cannot be reached. For decreasing S (Fig. 3c, d), shot noise becomes intense enough to overcome this overlap and inter-spike intervals corresponding to one period of the signal emerge and become more and more frequent. This fact leads to the smooth valley observed in CV within the range 1 μm^2 $<S<$ 10 μm^2. When lowering S below 0.1 μm^2 (Fig. 3e, f), the signal loses control of the spiking activity because of the increasing intensity of shot noise, and the inter-spike intervals tend to concentrate around a time slightly lower than 0.02 s, associated to the refractory period of the spikes and not to the period of the signal. This is confirmed by the fact that the ISIH found in the absence of any excitation current, when only shot noise can induce spiking activity, is very similar to that found in the presence of the signal. This situation is illustrated in Fig. 3f for $S=0.003$ μm^2, in coincidence with the optimal value of CV [Fig. 2].

In addition to the time behavior of V_m, its spectral analysis can provide useful information about the influence of shot noise. To this end, in Fig. 4 we show the spectral density of the fluctuations of V_m, $S_{Vm}(f)$, for several values of S in the absence of any excitation current. For $S>0.1$ μm^2, when shot noise is not intense enough for the appearance of spontaneous spikes (Fig. 3a–c), $S_{Vm}(f)$ exhibits a maximum at around 70 Hz, which, interestingly, may reveal the existence of intrinsic rhythmic oscillations in V_m [31], in this case induced by the presence of shot noise. Such oscillations are somehow visible in Fig. 1a for S= 1 μm^2. $S_{Vm}(f)$ presents a low-frequency plateau before the maximum and a dependence close to f^{-2} beyond it. In all the frequency range under analysis, $S_{Vm}(f)$ linearly scales with $1/S$ for $S>0.1$ μm^2. This behavior changes for $S\approx0.1$ μm^2, when the system size is at the limit for the emergence of spontaneous spikes. In these conditions, at the onset of the instabilities leading to the peaks in V_m, the noise increases significantly; indeed, more pronouncedly than $1/S$ except at the higher frequencies. Noticeably, the maximum around 70 Hz covers a wider frequency range. This change in shape preludes the frequency dependence exhibited by $S_{Vm}(f)$ for $S\leq0.01$ μm^2, when shot noise induces more and more frequent voltage spikes. In this range of S values (Fig. 3e, f), the maximum in $S_{Vm}(f)$ is mostly associated to the refractory period, and thus shifted around 50 Hz, and the values of the spectral density tend to become independent of S, except at the higher frequencies. The corresponding variance of V_m, shown in the inset of Fig. 4, which accounts for the noise at all the frequencies, reflects the described dependence on S.

The described frequency behavior of the V_m fluctuations originated by shot noise is similar to that found when other noise sources like channel and thermal noise are considered, both in the presence and absence of spontaneous spikes [31]. This fact indicates that the behavior of $S_{Vm}(f)$ is greatly determined by the presence or absence of spikes, and scarcely by the noise source at their origin. Remarkably, significant features around frequencies similar to those of the maximum observed here in $S_{Vm}(f)$ have been found in both experiments [32] and other numerical calculations [23]. On the

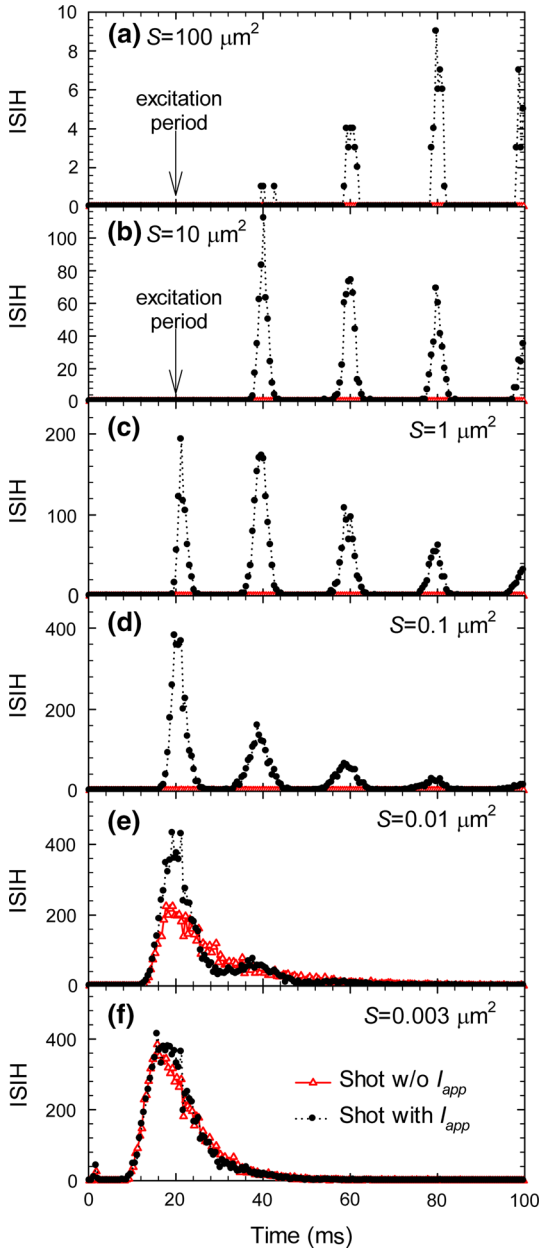

Fig. 3 ISIH for a sinusoidal excitation with $I_A = 1.5\ \mu A/cm^2$ and $f = 50$ Hz when ion shot noise is considered as the only noise source in the system, for **a** $S = 100\ \mu m^2$, **b** $S = 10\ \mu m^2$, **c** $S = 1\ \mu m^2$, **d** $S = 0.1\ \mu m^2$, **e** $S = 0.01\ \mu m^2$ and **f** $S = 0.003\ \mu m^2$. In **a** and **b**, the time corresponding to one period of the applied signal is indicated for clarity. The case $I_{app} = 0$ is also plotted for comparison

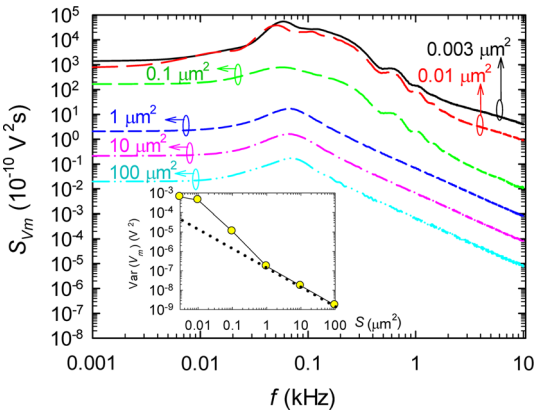

Fig. 4 $S_{Vm}(f)$ in the absence of I_{app} when ion shot noise is the only noise source considered in the system for several values of S. Inset: Variance of V_m as a function of S. (The dotted line shows the $1/S$ dependence)

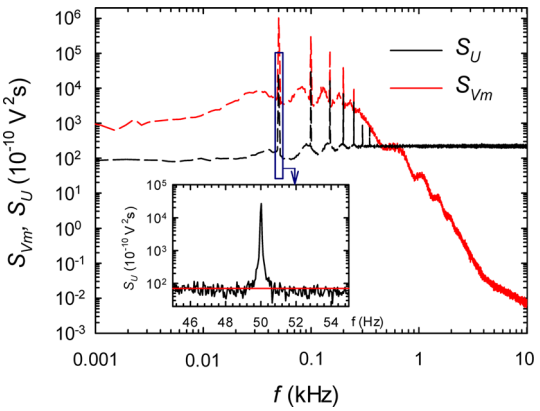

Fig. 5 $S_U(f)$ and $S_{Vm}(f)$ for a sinusoidal excitation of $I_A = 1.5\ \mu A/cm^2$ and $f = 50$ Hz when ion shot noise is the only noise source considered in the system. $S = 1\ \mu m^2$. Inset: $S_U(f)$ around 50 Hz, with the red line indicating the background value

other hand, the increase in the noise at the onset of instabilities is observed in other physical systems, like electronic devices, for example in Gunn diodes [33].

As shown before, the presence of an excitation current I_{app} like that considered in Fig. 3 makes possible the appearance of spikes originated by shot noise for values of $S > 0.1\ \mu m^2$, otherwise not present. Figure 5 presents $S_{Vm}(f)$ and $S_U(f)$ under such conditions ($I_A = 1.5\ \mu A/cm^2$ and $f = 50$ Hz), for $S = 1\ \mu m^2$ (Fig. 3c). Let us recall that $V_m(t)$ tracks the dynamics of the membrane voltage (including spikes), while $u(t)$ is just related to the presence/absence of spikes. Both $S_{Vm}(f)$ and $S_U(f)$ contain sharp peaks localized at multiples of the driving frequency due to the emerged voltage spikes [and also to the subjacent voltage response to the external sinusoidal current in the case of $S_{Vm}(f)$ (Fig. 1b)]. Remarkably, apart from the mentioned peaks, the shape and values of $S_{Vm}(f)$ at the lower frequencies are rather similar to those found for smaller patch sizes when spikes emerge in the absence of I_{app}, indicating, again, a common behavior related to the presence of spikes. However, beyond 1 kHz, significant differences are observed in the frequency roll-off, which is much stronger in the presence of the excitation. On the other hand, such a roll-off is absent in $S_U(f)$, since $u(t)$ corresponds to a spike train sequence given by δ-functions [Eq. (4)].

Since the neural information is encoded in the action potential spikes, the SNR is calculated in terms of $u(t)$ as the ratio between the peak value of $S_U(f)$ at the driving fre-

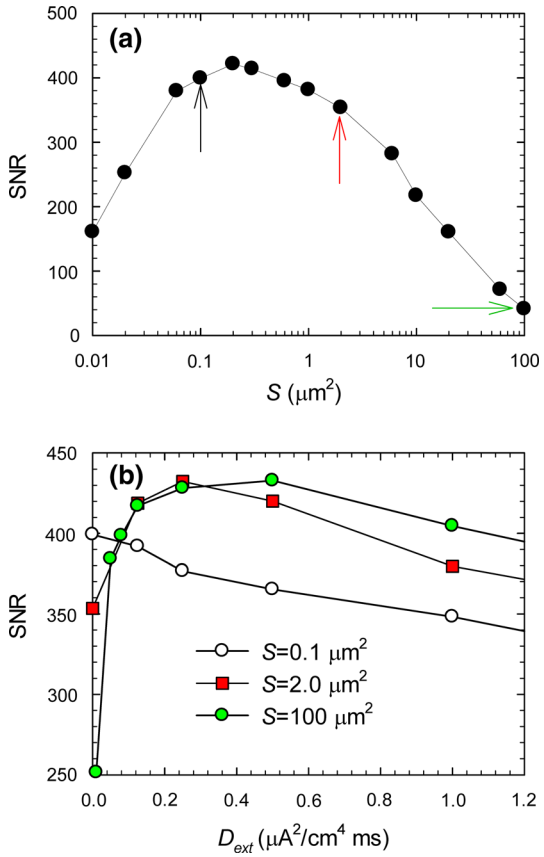

Fig. 6 SNR for a sinusoidal excitation of $I_A = 1.5\ \mu A/cm^2$ and $f = 50$ Hz **a** as a function of S when ion shot noise is the only noise source considered in the system, and **b** as a function of D_{ext} and for different values of S when ion shot noise is in competition with external noise

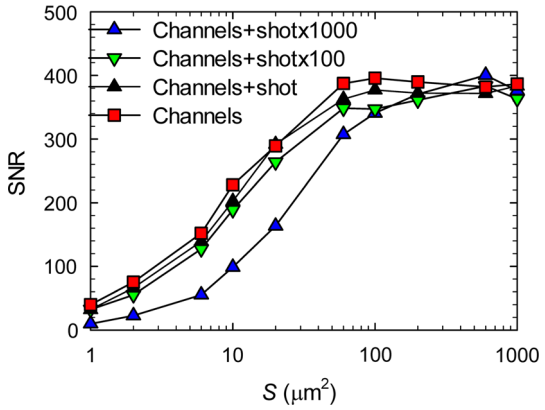

Fig. 7 SNR for a sinusoidal excitation with $I_A = 1.5\ \mu A/cm^2$ and $f = 50$ Hz as a function of S when considering ion shot noise in competition with channel noise. The cases in which ion shot noise is artificially amplified by 10^2 and 10^3 are also plotted for comparison, as well as the case in which only channel noise is present

quency, minus its background value and such a background value, as illustrated in the inset of Fig. 5. The SNR is plotted in Fig. 6a as a function of S. The total simulation time is 300 s. Significantly, ion shot noise leads to intrinsic SR, i.e., the response of the system to the external sinusoidal signal presents an optimal value in terms of the membrane patch size S, associated to the level of internal shot noise. For the considered periodic I_{app}, SNR presents maximum values of around 420 for S approximately 0.2 μm^2. For $S < 0.2\ \mu m^2$, the increasing shot noise deteriorates the system response. Under this circumstances, the addition of an external noise cannot further improve the SNR, and extrinsic SR cannot appear, as observed for $S = 0.1\ \mu m^2$ in Fig. 6b when adding an increasing dose of external noise D_{ext}. On the contrary, for $S > 0.2\ \mu m^2$, when SNR decreases due to the less intense shot noise, the addition of external noise leads to standard (extrinsic) SR behavior, as evidenced in Fig. 6b for the cases $S = 2\ \mu m^2$ and $S = 100\ \mu m^2$. The optimal SNR takes slightly higher values and appears for higher D_{ext} for increasing S.

We have shown that shot noise by itself can lead to a rich phenomenology in the noise behavior of the membrane voltage. However, in a real situation it competes with other noise sources like channel noise, that, being more intense, can conceal the described effects. Figure 7 presents the values of SNR as a function of S when ion shot noise is considered in competition with ion channel noise, in the absence of external noise. As observed, ion channel noise dominates, masking the effect of ion shot noise. Only if shot noise is amplified by more than two orders of magnitude, its influence on SNR becomes noticeable. Nevertheless, even though it cannot be detected in terms of SNR, the time scales involved in these noise sources are very different [27], and their influence on the membrane voltage fluctuations could become visible in different frequency ranges.

4 Conclusions

Intrinsic coherence, noise spectra and SR related to ion shot noise in excitable cell membrane patches have been investigated in terms of the system response to an applied sinusoidal signal below but very close to the onset of spikes. CV takes values under the unity for $S < 100\ \mu m^2$, denoting a correlation in the stochastic sequence of spikes. For $1\ \mu m^2 < S < 10\ \mu m^2$, CV presents a smooth valley of values around 0.6 in coincidence with the appearance of inter-spike intervals corresponding to one period of the excitation signal. The spectra of membrane voltage fluctuations show a common signature of the presence of spikes under different operating conditions, even in the absence of excitation, evidenced as a noticeable increase in the noise at the lower frequencies.

Significantly, ion shot noise shows intrinsic SR in terms of S when it is the only noise source considered in the system. Under this condition, SNR presents maximum values for S around 0.2 μm^2. For higher S, when the ion shot noise level

is lower than its optimal value, the standard extrinsic SR is observed by adding external noise.

References

1. Eisenberg, B.: Ion channels as devices. J. Comput. Electron. **2**, 245–249 (2003)
2. Ha, S.D., Ramanathan, S.: Adaptive oxide electronics: a review. J. Appl. Phys. **110**(1–20), 071101 (2011)
3. Kaneko, Y., Nishitani, Y., Ueda, M.: Ferroelectric artificial synapses for recognition of a multishaded image. IEEE Trans. Electron. Dev. **61**, 2827–2833 (2014)
4. Pershin, Y.V., Di Ventra, M.: Experimental demonstration of associative memory with memristive neural networks. Neural Netw. **23**, 881–886 (2010)
5. Prezioso, M., Merrikh-Bayat, F., Hoskins, B.D., Adam, G.C., Likharev, K.K., Strukov, D.B.: Training and operation of an integrated neuromorphic network based on metal-oxide memristors. Nature **512**, 61–64 (2015)
6. Romeo, A., Dimonte, A., Tarabella, G., D'Angelo, P., Erokhin, V., Iannotta, S.: A bio-inspired memory device based on interfacing Physarum polycephalum with an organic semiconductor. APL Mater. **3**(1–6), 014909 (2015)
7. Sourikopoulos, I., Hedayat, S., Loyez, C., Danneville, F., Hoel, V., Mercier, E., Cappy, A.: A 4-fJ/spike artificial neuron in 65 nm CMOS technology. Front. Neurosci. **11**(1–4), 123 (2017)
8. Chua, L.: Memristor, Hodgkin–Huxley and edge of chaos. IOP Nanotechnol. **24**(1–14), 383001 (2013)
9. Chein, W.R., Midtgaard, J., Shepherd, G.M.: Forward and backward propagation of dendritic impulses and their synaptic control in mitral cells. Science **278**, 463–467 (1997)
10. Hodgkin, A.L., Huxley, A.F.: A quantitative description of membrane current and its application to conduction and excitation in nerve. J. Physiol. **117**(4), 500–544 (1952)
11. Collins, J.J., Imhoff, T.T., Grigg, P.: Noise-enhancement tactile sensation. Nature **383**, 770 (1996)
12. Simonotto, E., Riani, M., Seife, C., Roberts, M., Twitty, J., Moss, F.: Visual perception of stochastic resonance. Phys. Rev. Lett. **78**, 1186–1189 (1997)
13. Hidaka, I., Nozaki, D., Yamamoto, Y.: Functional stochastic resonance in the human brain: noise induced sensitization of baroreflex system. Phys. Rev. Lett. **85**, 3740–3743 (2000)
14. Toghraee, R., Mashl, R.J., Lee, I.K., Jakobsson, E., Ravaioli, U.: Simulation of charge transport in ion channels and nanopores with anisotropic permittivity. J. Comput. Electron. **8**, 98–109 (2009)
15. Van der Straaten, T.A., Kathawala, G., Trellakis, A., Eisengerg, R.S., Ravaioli, U.: BioMOCA—a Boltzmann transport Monte Carlo model for ion channel simulation. Mol. Simul. **31**, 151–171 (2005)
16. Hwang, H., Schatz, G.C., Ratner, M.A.: Kinetic lattice grand canonical Monte Carlo simulation for ion current calculations in a model ion channel system. J. Chem. Phys. **127**(1–10), 024706 (2007)
17. Corry, B., Hoyles, M., Allen, T.W., Walker, M., Kuyucak, S., Chung, S.-H.: Reservoir boundaries in Brownian dynamics simulations of ion channels. Biophys. J. **82**, 1975–1984 (2002)
18. Boda, D., Busath, D.D., Eisenberg, B., Henderson, D., Nonner, W.: Monte Carlo simulations of ion selectivity in a biological Na channel: charge–space competition. Phys. Chem. Chem. Phys. **4**, 5154–5160 (2002)
19. Vasallo, B.G., Pardo-Galán, F., Mateos, J., González, T., Hedayat, S., Hoel, V., Cappy, A.: Stochastic model for action potential simulation including ion shot noise. J. Comput. Electron. **16**, 419–430 (2017)
20. Schmid, G., Goychuk, I., Hänggi, P.: Stochastic resonance as a collective property of ion channel assemblies. Europhys. Lett. **56**, 22–28 (2001)
21. Schmid, G., Goychuk, I., Hänggi, P.: Channel noise and synchronization in excitable membranes. Phys. A **325**, 165–175 (2003)
22. Schmid, G., Goychuk, I., Hänggi, P., Zeng, S., Jung, P.: Effect of channel block on the spiking activity of excitable membranes in a stochastic Hodgkin–Huxley model. Phys. Biol. **1**, 61–66 (2004)
23. Adair, R.K.: Noise and stochastic resonance in voltage-gated ion channels. PNAS **100**, 12099–12104 (2003)
24. Faisal, A.A., White, J.A., Laughlin, S.B.: Ion-channel noise places limits on the miniaturization of the brain's wiring. Curr. Biol. **15**, 1143–1149 (2005)
25. Faisal, A.A., Selen, L.P.J., Wolpert, D.M.: Noise in nervous systems. Nature Rev. **9**, 292–303 (2008)
26. Läuger, P.: Shot noise in ion channels. Biochim. Biophys. Acta **413**, 1–10 (1975)
27. Brunetti, R., Affinito, F., Jacoboni, C., Piccinini, E., Rudan, M.: Shot noise in single open ion channels: a computational approach based on atomistic simulations. J. Comput. Electron. **6**, 391–394 (2007)
28. Schroeder, I., Hansen, U.-P.: Interference of shot noise of open-channel current with analysis of fast gating: patchers do not (yet) have to care. J. Membr. Biol. **229**, 153–163 (2009)
29. Gillespie, D.T.: A general method for numerically simulating the stochastic time evolutions of coupled chemical reactions. J. Comput. Phys. **22**, 403–434 (1976)
30. Gillespie, D.T.: Exact stochastic simulation of coupled chemical reactions. J. Phys. Chem. **81**, 2340–2361 (1977)
31. Kuang, S., Wang, J., Zeng, T.: Intrinsic rhythmic fluctuation of membrane voltage evoked by membrane noise in the Hodgkin–Huxley system. Acta Phys. Pol. A **117**, 435–438 (2010)
32. Fishman, H.M., Poussart, D.J., Moore, L.E.: Noise measurements in squid axon membrane. J. Membr. Biol. **24**, 281–304 (1975)
33. García-Pérez, O., Alimi, Y., Song, A., Íñiguez-de-la-Torre, I., Pérez, S., Mateos, J., González, T.: Experimental assessment of anomalous low-frequency noise increase at the onset of Gunn oscillations in InGaAs planar diodes. Appl. Phys. Lett. **105**(1–4), 113502 (2014)